FIRST BEAM CHARACTERIZATION OF SRF GUN II WITH A COPPER PHOTOCATHODE

J. Teichert#, A. Arnold, P. Michel, P. Murcek, R. Xiang, HZDR, Dresden, Germany
P. Lu, H. Vennekate, TU Dresden & HZDR, Dresden, Germany

Abstract

An improved SRF gun (ELBE SRF Gun II) has been installed and commissioned at HZDR. This new gun replaces the first SRF gun at the superconducting linear accelerator ELBE which had been in operation since 2007. The new SRF gun II has an improved 3.5-cell niobium cavity and a superconducting solenoid is integrated into the gun cryostat. The first beam test has been carried out with a Cu photocathode. Using the standard high repetition rate laser system, this delivers low bunch charges of a few pC only. The beam parameters for this low charge beam have been measured, and the first beam has been guided into the ELBE accelerator.

INTRODUCTION

A high-brightness electron source is one of the key elements of an energy recovery linac (ERL) as it has been proposed for future light sources, or other application in high energy particle physics. Since ERLs are usually designed for high current and continuous wave (CW) operation, their electron sources require both properties: low emittance and high average current. At present, there are three electron source types in operation at ERLs or their application is planned: electron sources with a static high voltage (DC guns), normal conducting radio frequency (RF) electron sources, and superconducting RF electron sources (SRF guns). All three types are photoelectron injectors utilizing powerful lasers and photo cathodes for electron beam generation. DC guns present the most developed technology and have demonstrated high repetition rate and high average current operation at several CW accelerators. The DC gun of the Cornell injector holds the world record in CW current and in transverse emittance [1, 2], and recently the specifications for CLRS could be successfully demonstrated [3]. SRF guns are still in the development phase but they offer the potential of significant higher acceleration fields and should therefore be able to deliver smaller emittances for high bunch charges [4].

THE ELBE SRF GUN II

In May 2014 the second SRF gun (ELBE SRF Gun II) was installed at the ELBE superconducting linear accelerator facility. The basic design of this new gun is similar to that of the former SRF Gun I [5], but it has a new 3.5-cell cavity made of fine grain niobium. Beside several smaller modifications, the new cavity has a different acceleration field distribution, i.e. a peak field ratio of 80% to 100% between half-cell and TESLA cells.

#j.teichert@hzdr.de

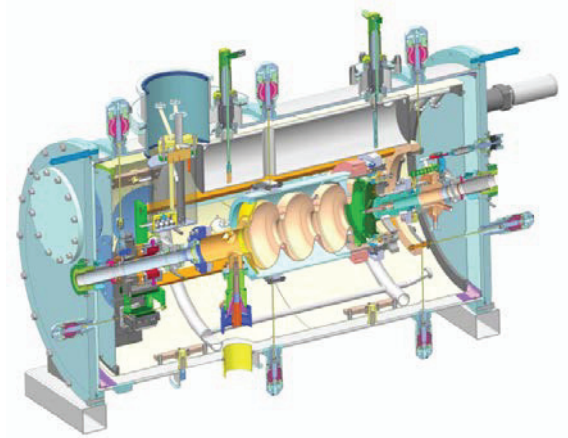

Figure 1: CAD view of the SRF Gun II cryomodule.

Benefit from a higher gradient, beam dynamic simulation showed reduced emittance and bunch length.

The design of the new cryomodule for SRF gun II is shown in Fig. 1. The 1.3 GHz Nb cavity consists of three TESLA cells and a specially designed half-cell. Another superconducting cell, called choke filter, prevents the leakage of the RF field towards the cathode support system. A normal conducting (NC) photocathode is installed in this system, which is isolated from the cavity by a vacuum gap and cooled with liquid nitrogen.

A new feature is the integration of a superconducting SC) solenoid in the cryomodule for emittance preservation purposes. Compared to the NC solenoid of SRF gun I which was placed downstream of the gun, the new design is much more compact and the distance to the cathode is smaller. The SC solenoid is placed on a remote-controlled x-y table to align its center to the electron beam axis. The cryogenic design of the assembly is sophisticated: The solenoid is cooled with 2 K He by means of a bypass from the cavity. The in-vacuum step motors and translation tables are on 77 K to reduce the heat load to the liquid He bath. Additional μ-metal shields keep the solenoid remanence field and the step motors fields on a 1 μT level near the cavity. Details of the SC solenoid design and testing are published in ref. [6].

Compared to the primary setup of SRF Gun I described in [5] there are several modification in the RF system of the gun. Now the RF main power with a frequency of 1.3 GHz is delivered by a solid state amplifier with a CW power of 10 kW [7]. The previous plastics (Rexolite) warm window is replaced by a fused silica window with higher thermal stability. A three stub tuner in the wave guide allows a variation of the band width. The analog low-level RF control system und the coaxial ELBE main power coupler with fixed coupling are still in use.

ISBN 978-3-95450-183-0

The drive laser for the SRF gun is a two-channel system developed by MBI Berlin and can deliver both laser pulses at 13 MHz with 3 ps FWHM and at 500 kHz (optionally 250 and 100 kHz) with 10 ps FWHM. These two channels support the two planned operation modes of the SRF gun. Both channels produce temporally Gaussian shaped pulses, and the average power at 258 nm can reach about 1 W. The laser consists of a Nd:glass oscillator at 52 MHz, a pulse picker generating the 13 MHz with an electro-optical modulator, a fiber-laser preamplifier for the 13-MHz-channel, a regenerative preamplifier for the 500-kHz-channel, a multipass final amplifier for both channels, and two frequency conversion stages with LBO and BBO crystals. The laser spot is transversally shaped to a round flat-top by an aperture on the laser table and then imaged onto the photo cathode with a four-lens telescopic system.

For the electron beam characterization the existing diagnostics beamline [8] has been utilized. An insertable Faraday cup delivers the beam current, five screen stations equipped with YAG(Ce) screens serve for beam profile measurements, and a 180° dipole magnet is used for energy and energy spread measurements. For transverse phase space measurements a movable slit scan system is installed.

MEASUREMENTS

Cavity Performance

Cavity performance results for the ELBE SRF Gun II together with a comparison to SRF Gun I are presented in Fig. 2. After commissioning of the gun and several checks, RF measurements in August 2014 give an intrinsic quality factor of $>10^{10}$ and a maximum acceleration gradient in CW of 10 MV/m (25.6 MV/m peak field) was obtained. More details of the RF related measurements and results of performance tests of components are published in ref. [9]. In the following commissioning period electron beam was produced with the Cu photocathode with acceleration gradients up to 9 MV/m. Later the photocathode transfer system was installed and Cs_2Te photocathodes were prepared. A first test with a Cs_2Te photocathode was performed in February 2015. Unfortunately it turned out after insertion that this photocathode was bad, i.e. the quantum efficiency was very low and very strong field emission was observed, increasing the He consumption as well as the dark current. The bad photocathode was taken out and the performance of the cavity was measured again. It was found that the cavity had been polluted. The helium consumption due to field emission was still significantly higher than before and the same for the dark current. A high power RF processing of the cavity could reduce the dark current but did not improve the cavity performance. Thus in the following beam time the acceleration gradient was restricted to 7 MV/m.

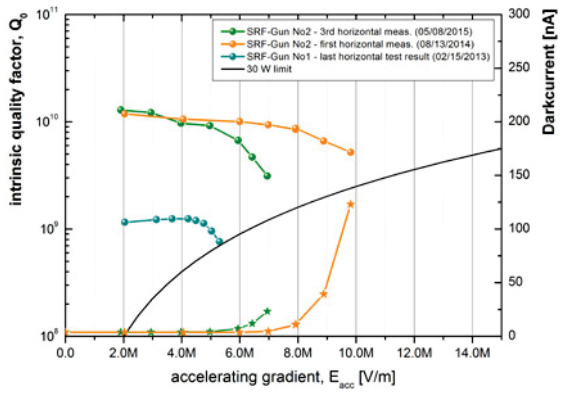

Figure 2: Measured cavity performance of ELBE SRF Gun II (intrinsic quality factor versus acceleration gradient) and comparison with the previous SRF Gun I.

Gun and Laser Parameter

Electron beam was produced and characterized in CW with acceleration gradients of 6, 7, 8, and 9 MV/m which belong to peak fields from 15.5 to 23 MV/m. The photo cathode was biased with a DC voltage of -5 kV. The dark currents during measurements were about 50 nA or less.

The photocathode was solid, polycrystalline Cu which was mirror-like polished. Before assembled in the vacuum it was dipped in citric acid and cleaned with acetone. A further in-situ processing, like laser cleaning, was not carried out. A quantum efficiency of about $2x10^{-5}$ was measured. Thus CW beam currents between 3 and 300 nA were produced and the corresponding maximum bunch charge was 3 pC at 100 kHz pulse repetition rate.

The UV drive laser at 258 nm wave length had a power between 200 and 800 mW on the laser table. Due to the cutting aperture, vacuum window, and mirror losses the laser power at the cathode was about 5 – 10% of this value. The transverse flat-top laser was adjusted to 1 and 2 mm diameter on the cathode, and the longitudinal profile was Gaussian with 3 ps FWHM (13 MHz) or 10 ps FWHM (100 kHz).

Beam Based Alignment

Laser Phase Scan: The alignment procedure start with the fixing of the laser pulse arrival time at the cathode with respect to the RF phase which is called the laser phase in the following and measured in degrees of the RF wave. For the RF time-dependence we assume a sine function $E_z(z,t) = E_0(z)\sin(2\pi f_{RF}t + \phi_l)$ with the laser phase ϕ_l and the center of the laser pulse arrives the cathode at t = 0. In the measured phase scan, presented in Fig. 3, in which the beam current is measured using a Faraday cup about 0.5 m downstream the gun, the left-side slope defines the zero value of ϕ_l, since for $\phi_l<0$ the RF field direction is inverse and electrons are not emitted. The phase width in the current increase is determined by the laser pulse length und further broadened by phase jitter or other instabilities. The DC bias of the cathode shifts the slope to lower laser phase values. Therefore the bias was switched off for the laser scan curve used for calibration.

ISBN 978-3-95450-183-0

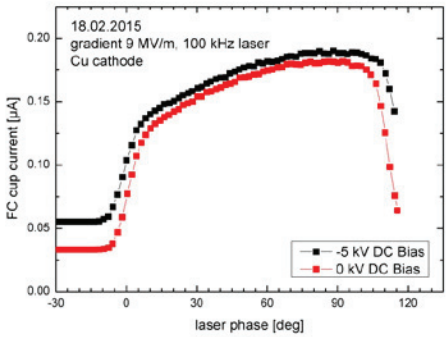

Figure 3: Laser phase scan for phase for zero-point adjustment.

Adjustment of Laser Spot on Photocathode: The next step of the alignment procedure was to center the laser spot on the cathode. The method we used is similar to a current scan for solenoid or quadrupole alignment. But the scan variable is the laser phase and the position of the electron beam spot on a screen downstream is observed. All optical components between the cavity and the screen, i.e. the solenoid, the quadrupoles, the dipole and the correction coils were switched off. The laser spot was moved across the photocathode in horizontal and vertical direction in order to find the position, where the phase scan caused the minimal beam spot shift on the screen. Figure 4 shows the results of the alignment. Beginning with the initial position of the laser spot (in black) with coordinates (0,0) on the virtual cathode, the laser spot was changed to the position (-0.2 mm, 0.8 mm) giving the minimal shift of the electron beam with laser phase. The accuracy of the laser spot alignment is about 100 µm.

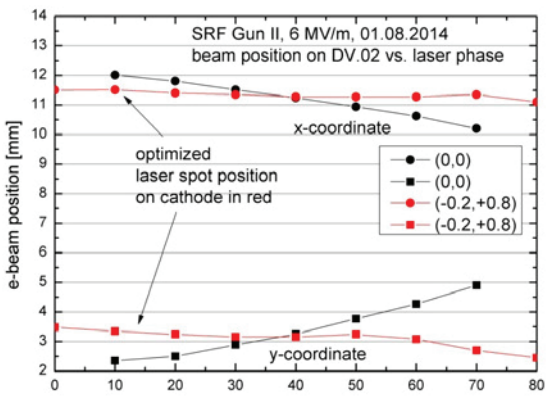

Figure 4: Laser spot centering on the photo cathode. For different laser spot positions the beam position on screen DV02 was measured as function of the laser phase.

Cavity Alignment: During installation the cryomodule of the SRF gun was mechanically aligned in the warm state with respect to the existing ELBE accelerator beam lines considering the shrinking of the cold mass after cool-down. Nevertheless a misalignment was found guiding the electron beam through the first beamline section with the quadrupole triplet. Assuming that the triplet defines the beam line axis, a difference up to 3 mm between the electron beam defining the gun cavity axis and the beam line axis at the quadrupole was found. By means of the beam corrector coils, the screens upstream and downstream the quadrupoles, and by scanning the quadrupole currents, it was possible to determine the differences in position and tilt between these two axes. Then the cavity position and tilt were corrected by the micrometer movers at the gun cryomodule. Repeating this process of cavity realignment and beam based measurement several times, an agreement between the two axes with an accuracy of 50 µm was achieved.

Solenoid Alignment: The SC solenoid can be moved remotely controlled in horizontal and vertical direction with step motors. As the laser spot is centred on the cathode, the electron beam axis defines the target for the solenoid alignment. The solenoid is first switched off and then excited with the nominal current, the centre positions on the first view screen is measured, and the solenoid moved until both positions agreed. Since the beam spot moves on a small circular path when the current is increasing, it seems that there is still a small angle misalignment of the solenoid which cannot be corrected.

Beam Parameter Measurement

Beam Energy and Energy Spread: The energy and energy spread of the beam was measured with the 180° dipole magnet in the diagnostics beamline [7]. The arrangement of the screens DV04 in forward direction downstream the dipole and DV05 in the 180°-direction allows a beam spot size correction of the energy spread measurement, and thus to measure up to very small values. The kinetic energy as function of laser phase for different acceleration gradient is presented in Fig. 5. With increasing gradient the energy maximum in the curves moves towards higher laser phases. Since the gun´s working point is near to this maximum, a higher gradient act twofold on the electron launch field strength. The slope of the curve determines the correlated energy spread produced by the gun.

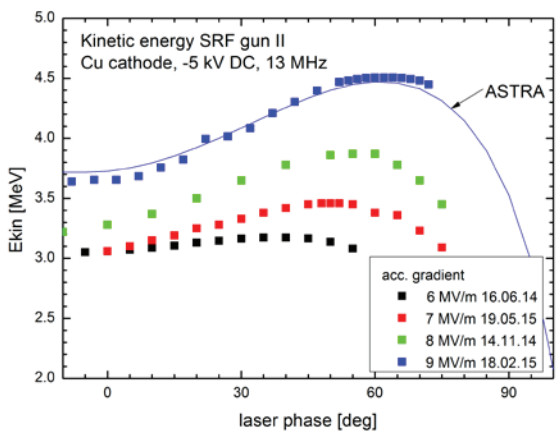

Figure 5: Kinetic energy as function of the laser phase for different acceleration gradients.

ISBN 978-3-95450-183-0

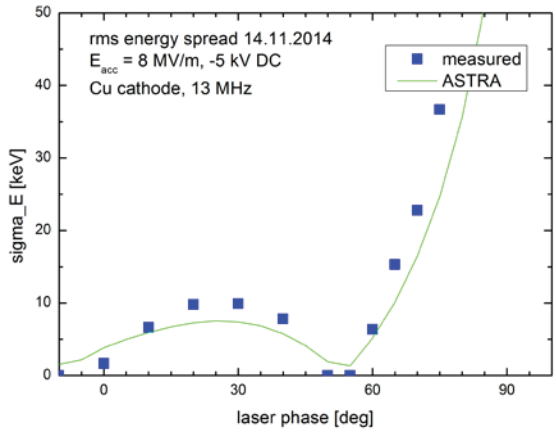

Figure 6: Results of the rms energy spread vs. laser phase for short-pulse laser (3 ps FWHM).

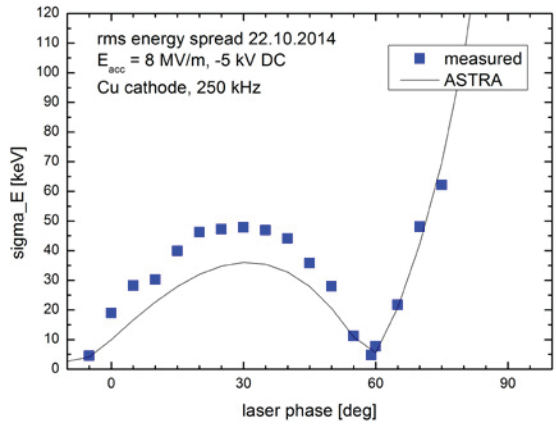

Figure 7: Results of the rms energy spread vs. laser phase for long-pulse laser (10 ps FWHM).

In the case of very low bunch charge, the energy spread is proportional to $dE/d\phi_1$ and to the laser pulse length as the measured curves show in Figs. 6 and 7. The sign of the correlated energy spread is like that the bunch has a high energy tail for the smaller laser phases. The long pulse laser, Fig. 7, produces an about five times higher energy spread than the shorter one. The discrepancy with respect to the ASTRA simulation can be caused by an in reality about 20% longer laser pulse than it was specified.

Transverse Emittance: The transverse emittance measurements were carried out using the quadrupole scan and the moving slit scan technique. Results of both measurements are shown in Fig. 8 for a laser spot between 1 mm and 1.5 mm in vertical and horizontal direction. In general, there are three contributions to the total emittance: thermal emittance, RF field effects, and space charge effects. Here the RF field effect is small and the space charge effect is negligible. The dominant thermal emittance is proportional to the rms laser spot size and in a wide range independent of the laser phase as it is predicted by the ASTRA simulation.

Bunch Length: First results of the bunch length were obtained applying the phase scan method. Thereto the beam from the gun was guided through the dogleg beamline section into the first linac module of the ELBE accelerator. In the module the phase of the second cavity C2 was modulated and the following first chicane magnet together with a YAG screen in the 45°-beamline serve as energy spectrometer. The phase scan method has been described in [10].

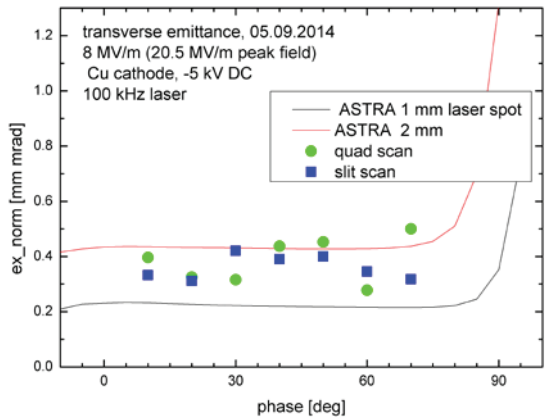

Figure 8: Results of the transverse emittance from moving slit scan method (vertical) and quadrupole scan (horizontal).

Figure 9 presents the ASTRA simulation for the long pulse laser (10 ps FWHM, 100 kHz) and for the short pulse laser (3 ps FWHM, 13 MHz), as well as the measurement values for the short pulse laser at different laser phases. As it can be seen from the simulation the bunch length increases with the laser phase monotonously. Therefore the shortest bunch length appears near to zero laser phase, where indeed a value of 480 fs was measured. The results are preliminary and a correction with respect to beam transport effects from the gun to the linac, especially due to the R_{56} of the dogleg and the drift ($1/\gamma^2$-term), is still required.

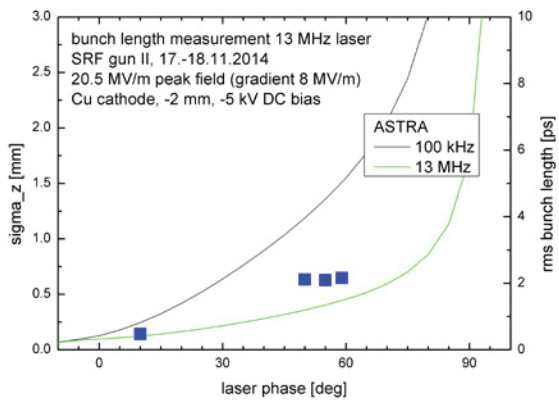

Figure 9: ASTRA results for the rms bunch length vs. laser phase for the 10 ps laser (100 kHz) and the 3 ps laser (13 MHz) and experimental results for the 3 ps laser obtained with the cavity phase scan method.

Dark Current

For normal conducting RF photo injectors dark current is a serious issue and previous results indicate that the mitigation of dark current requires attention for SRF guns too [11]. The sources of dark current are field emitters

ISBN 978-3-95450-183-0

within the cavity field of the gun which produce electrons escaping the gun. Depending on its properties the dark current can partially gain energy in the accelerator and can be further transported through its beamlines producing beam loss, can increase the measurement background of experiments, or can damage accelerator components. A typical picture of photo electron beam and dark current of the SRF Gun is shown in Fig. 10. For characterization of the dark current we measured its dependence on the acceleration gradient and its energy spectrum.

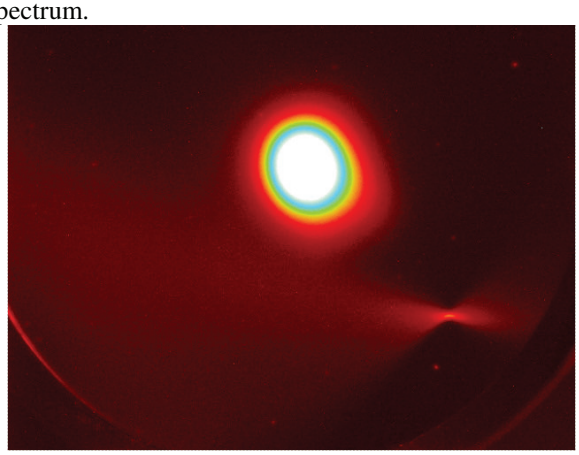

Figure 10: Screen image with photo electron beam spot (200 nA) and the dark current (53 nA) without any focusing by solenoid or quadrupole.

Figure 11 presents a comparison of the dark current for SRF gun II and the previous SRF gun I. Both measurements are performed for clean and polished metal cathodes without photo emission layers, e.g. the field emitters are situated at the cavity surface. It is visible that the onset of field emission is much higher for SRF gun II. At the working point of 18 MV/m the dark current is about 20 nA. The dark current spectrum, presented in Fig. 12, has one single dominant peak at 2.8 MeV whereas the kinetic energy of the photo current beam is at 3.6 MeV. This energy of the dark current is outside the energy acceptance of the dogleg. Still an open question is, to what extend the photo emission layers like Cs_2Te contribute to dark current.

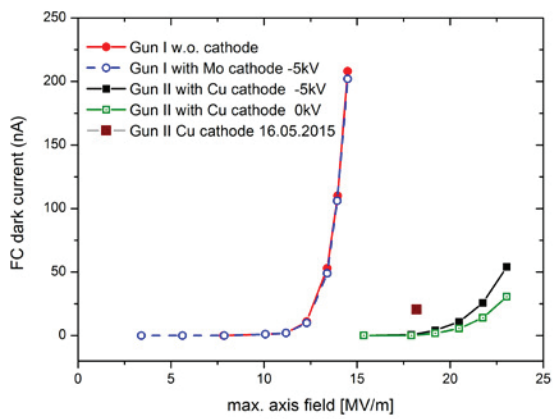

Figure 11: Comparison of dark current measurements as function of peak acceleration field for SRF Gun I and II.

Both results are for clean metallic photocathode without photo emission layers.

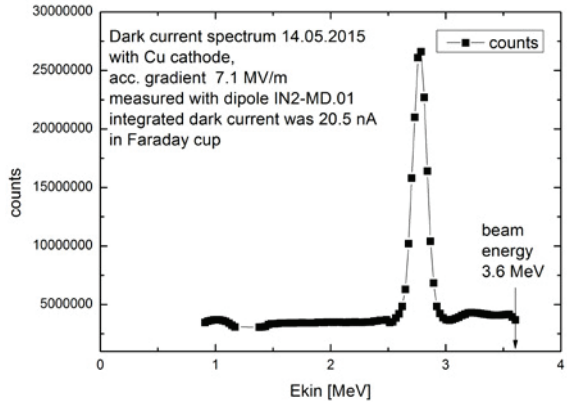

Figure 12: Dark current spectrum of SRF Gun II measured after the test with the bad Cs_2Te photo cathode.

SUMMARY AND OUTLOOK

The ELBE SRF Gun II has been commissioned and beam parameters have been measured with a copper photocathode. A first test with a Cs_2Te photocathode failed and polluted the cavity. Thus the future operation of the gun is limited to about 7 MV/m whereas an acceleration gradient of 10 MV/m was achieved in the first RF tests. The dark current measured to 20 nA is low enough that it will not disturb user operation.

Simulations with actual performance parameters of the SRF Gun II confirm that the gun will be useful for future user operation. Especially higher bunch charges up to 0.5 nC will improve the experimental prospects at ELBE. The crucial point at present is the quality and cleanness of photocathodes. The latest experiences showed that exchange of photocathodes exhibits the highest risk for cavity contamination.

ACKNOWLEDGMENT

We would like to thank the whole ELBE team for their help and assistance with this project. The work is supported by the European Community under the FP7programme (EuCARD-2, contract number 312453, and LA3NET, contract number 289191) and by the German Federal Ministry of Education and Research (BMBF) grant 05K12CR1.

REFERENCES

[1] C. Gulliford et. al., Phys. Rev. ST Accel. Beams 16, 073401 (2013).
[2] B. Dunham et. al., Appl. Phys. Lett. 102, 034105 (2013).
[3] C. Gulliford et. al., Appl. Phys. Lett. 106, 094101 (2015).
[4] A. Arnold and J. Teichert, Phys. Rev. ST Accel. Beams 14, 024801 (2011).
[5] A. Arnold et. al., Nucl. Instrum. Methods Phys. Res. A 577, 440 (2007).
[6] H. Vennekate et al., "Emittance Compensation for an SRF Photo Injector", Proceedings of SRF'13, Paris, France (2013).
[7] H. Büttig et al., Nucl. Instrum. Methods Phys. Res. A 704, 7 (2013).

ISBN 978-3-95450-183-0

[8] T. Kamps et al., Review of Scientific Instruments 79 (2008) 093301.
[9] A. Arnold et al., "Commissioning Results of the 2nd 3.5 Cell SRF Gun for ELBE", Proceedings of LINAC´14, Geneva, Switzerland (2014).
[10] D.H. Dowell et al., Nucl. Instrum. and Methods Phys. Res. A 507, 331 (2003).
[11] R. Xiang et al., Phys. Rev. ST Accel. Beams 17, 043401 (2014).

ISBN 978-3-95450-183-0